

Evolution from the coplanar to the perpendicular plane geometry of helium ($e, 2e$) differential cross sections symmetric in scattering angle and energy

A. J. Murray and F. H. Read

Department of Physics, Schuster Laboratory, Manchester University, Manchester, M13 9PL, United Kingdom

(Received 26 October 1992)

Experimentally determined differential cross sections are presented for the ($e, 2e$) process in helium, in which the two outgoing electrons have the same energy and the same scattering angle with respect to the incident beam. At four incident energies from 20 to 50 eV above the ionization threshold the detection plane defined by the outgoing electrons was varied from being coplanar with the incident beam to being perpendicular to the beam. The differential cross section evolves from a two-peak structure in coplanar geometry to a three-peak structure in the perpendicular plane. At the lowest energy the forward-scattering coplanar peak is smaller than the backscatter peak, in contrast to the results at higher energies. A deep minimum is seen at an intermediate plane angle of 67.5° , this minimum being deepest at 40 eV above the ionization threshold. The results are normalized to an absolute scale using previous coplanar measurements as discussed in the text. The spectrometer used to collect these results is fully computer controlled and real-time computer optimized.

PACS number(s): 34.80.Dp

I. INTRODUCTION

Angular-correlation experiments in which an incident electron ionizes a target atom and the resulting electrons are detected in coincidence provide exacting tests of current ionization theories [1], particularly for incident electron energies in the range from a few eV to about 100 eV above threshold. Ionization in this energy range involves all the complexities of exchange and capture, distortions in the incoming and outgoing channels, and short- and long-range correlations. Testing of these theories is further enhanced [2] by including a wide range of directions of the scattered and ejected electrons rather than restricting the experiments to either coplanar geometry or to the recently introduced perpendicular-plane geometry [3,4]. Results have recently been published close to threshold over a wider range of scattering directions [5], and it is the purpose of the present study to make detailed measurements in this energy region for a wide range of scattering directions.

The ($e, 2e$) process may be represented by

$$e_0 + A \rightarrow A^+ + e_a + e_b,$$

where e_0 indicates an incident electron with energy E_0 and momentum \mathbf{k}_0 , and e_a and e_b indicate that two outgoing electrons with energies E_a and E_b and momenta $\mathbf{k}_a(\theta_a, \phi_a)$ and $\mathbf{k}_b(\theta_b, \phi_b)$, respectively (Fig. 1). The parameters $E_0, E_a, \theta_a, \phi_a, E_b, \theta_b, \phi_b$ are experimentally selectable within the constraints that energy must be conserved. For an unpolarized target and incident electron beam the only azimuthal angle of significance is $\phi = \phi_a - \phi_b$.

Coplanar geometry is that in which ϕ is 0° (or 180°) and the perpendicular plane is that in which θ_a and θ_b are both 90° . In the experiments discussed here, the detection plane defined by the momenta of the outgoing elec-

trons is held constant in the laboratory frame and the angle ψ defined as the angle between the direction of the incident beam and the detection plane is varied (Fig. 2). Coplanar and perpendicular-plane geometries therefore correspond to $\psi = 0^\circ$ and 90° , respectively. The detected electrons are selected to have equal energy and equal angles ξ with respect to the projection of the incident electron momentum onto the detection plane. All geometries thus coincide at $\xi_a = \xi_b = 90^\circ$, allowing a convenient normalization point as the incident electron-beam angle ψ is varied.

The ($e, 2e$) differential cross sections are placed on an absolute scale by normalizing against previous coplanar measurements [6]. Since the detected electrons are symmetric in both scattering angle and energy, the cross section that is measured can be described as a differential cross section "doubly symmetric" in scattering angle and energy. This description will help to differentiate between the present experiments and later ones in which one or both of these symmetries are relaxed.

In the present experiments the doubly symmetric differential cross section has been measured using a heli-

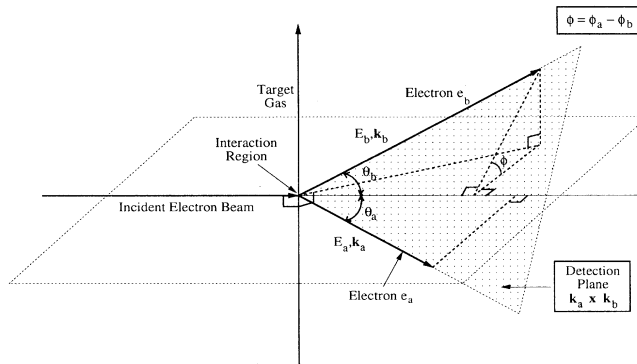


FIG. 1. The interaction region and detection plane defined with respect to the usual (θ, ϕ) coordinate geometry.

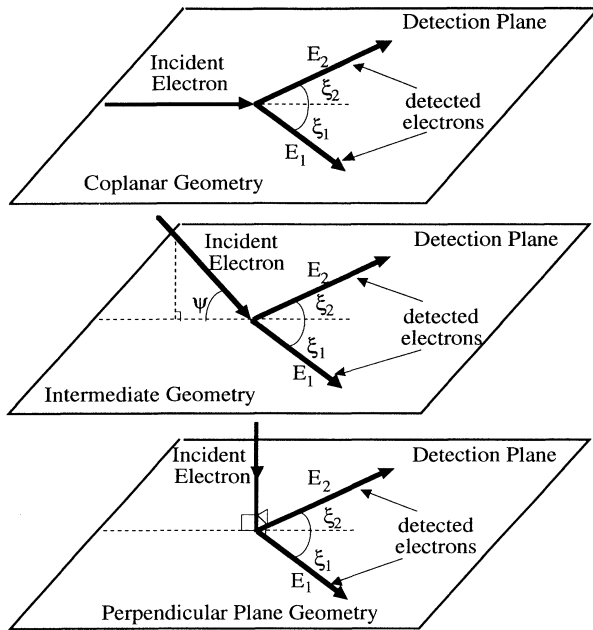


FIG. 2. The experimental geometry, showing the evolution from coplanar to perpendicular plane geometry [(a)–(c)]. ψ is defined as the angle between the detection plane and the direction of the incident electron beam. ξ is defined as the symmetric electron scattering angle in the detection plane.

um target with incident electron energies ranging from 20 to 50 eV above the ionization threshold, in steps of 10 eV. At the lowest incident energy, measurements were made for nine different gun angles [2], whereas at 30, 40, and 50 eV above threshold six different ψ angles were selected.

II. THE ELECTRON-COINCIDENCE APPARATUS

The electron-coincidence apparatus was designed to measure angular correlations between electrons emerging from electron-impact ionization in the range from 1 to 100 eV, and is capable of accessing all geometries from the coplanar to the perpendicular-plane geometry [2,3]. Initial experiments [4] were confined to the perpendicular-plane and were designed to test the near-threshold Wannier model [7]. Later experiments [3] were also confined to the perpendicular plane but the incident energy ranged up to 80 eV above threshold and the spectrometer was improved and configured to operate completely under computer control [8].

Figure 3 shows a schematic of the apparatus configured in the perpendicular plane. The spectrometer is mounted vertically on a stainless-steel flange supported in a cylindrical vacuum chamber pumped by a 500-l/s Balzers turbomolecular pump. Magnetic fields are reduced to less than 5 mG at the interaction region by μ -metal shields placed internally and externally, internal magnetic fields being avoided by manufacturing all components from either 310 stainless steel, molybdenum, or vacuum-compatible aluminum. All surfaces that the electrons approach are constructed from molybdenum, while the spectrometer mountings are 310 stainless steel.

The electron gun incorporates two triple-aperture elec-

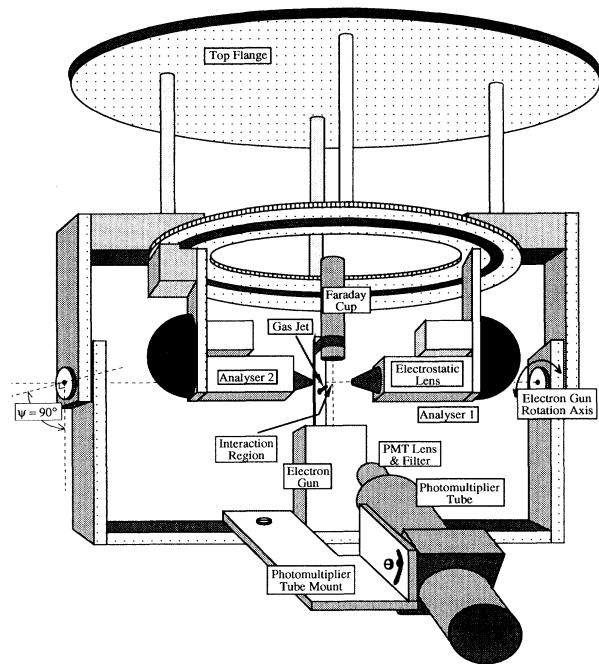


FIG. 3. The spectrometer configured in the perpendicular plane. The electron gun, Faraday cup, atomic beam source, and photomultiplier tube are constrained to move together as the gun angle ψ is changed.

trostatic lenses with intermediate-beam and pencil angle-defining apertures and has an energy resolution of approximately 600 meV. The electron energy is selectable from 20 to 300 eV and the gun is capable of supplying up to 4 μ A of current focused to a 1-mm-diameter beam at the interaction region, with zero beam angle and a pencil angle of approximately 2° as established using a SIMION electron trajectory program [3]. To facilitate focusing of the electron beam onto the interaction region, photons originating in this region are focused onto a bialkali photocathode photomultiplier tube via a lens, an aperture, and an optical filter that passes helium radiation at 450 ± 25 nm. This wavelength is chosen to allow the interaction volume to be accurately focused onto the photocathode by placing a light source in place of the photomultiplier tube behind the aperture and visibly back focusing this source onto the interaction region. The gun, the photomultiplier tube, the atomic beam source, and the Faraday cup are mounted so as to allow rotation from the coplanar to the perpendicular-plane geometry.

Two identical hemispherical deflection analyzers rotate in the horizontal detection plane. The analyzer input lenses are triple cylinder lenses of diameter 16.25 mm with object and image distances $P = Q = 4D$, having real entrance apertures of diameter 3.5 mm. These lenses were modeled using a SIMION ray tracing program and are found to have an acceptance half angle of approximately 3° over the range and resolution of scattering energies presented here. Following energy selection the electrons are detected by channel-electron multipliers. The analyzers are prevented from colliding with either the electron gun, the Faraday cup, or each other by position-sensing optical interrupters connected to the

external control electronics.

Internal electrical connections are via shielded PTFE coated advance (Constantin) wire, while the high-voltage supply lines are doubly shielded RG188A/U coaxial cables. The photomultiplier tube directly feeds an ORTEC 473A discriminator which drives an ORTEC 441 ratemeter. The channel-electron-multiplier pulses are amplified by Phillips Scientific 6954 100×400 ps rise-time preamplifiers located directly at the vacuum feedthroughs. These amplifiers feed ORTEC 473A constant-fraction discriminators placed in separate NIM crates to increase signal isolation. The analyzer count rates are monitored with ORTEC 441 ratemeters. The fast constant-fraction discriminator NIM pulses feed an ORTEC 437A time-to-amplitude converter via appropriate delay lines, the resulting 8ns full width at half maximum coincidence signal accumulating in an ORTEC multichannel analyzer. Coincidence count rates in the present experiments varied from 0.04 to 3 Hz.

Unique to this apparatus is the computer interface which controls and optimizes all aspects of the spectrometer from the tuning of the electron gun and analyzers to the setting of the analyzer positions and subsequent data collection. Briefly, at the heart of the system is an IBM 80286 PC which controls the spectrometer and receives all information from the system. The computer adjusts the spectrometer lens and deflector voltages, optimizing these to either electron-beam current, photomultiplier tube counts, or analyzer counts at regular intervals using a modified simplex technique based upon the method of Nelder and Mead [9]. The spectrometer runs unattended for continuous periods of typically one week, the results obtained being found to be more reliable and consistent than was previously possible with manual optimization. Full details of the computer control and optimization may be found in Ref. [8].

III. EXPERIMENTAL RESULTS AND DISCUSSION

A. The experimental procedure

Prior to data accumulation, the electron gun is set to the required gun angle ψ and the lenses and deflectors of the gun are computer optimized, first maximizing the Faraday cup current and then maximizing the photon counts as detected by the photomultiplier tube. This ensures that the electron current is steered and focused to a beam of diameter approximately 1 mm at the interaction region.

The analyzers are moved under computer control to their starting angles and their input electrostatic lenses and deflectors are computer optimized to their respective noncoincidence counting rates. A coincidence timing spectrum is then acquired for a predetermined time, after which the analyzers are moved to a new angle ξ in the detection plane. This optimization is repeated until the analyzers have swept around the available detection plane, at which point the whole system is reoptimized and the data-collection process repeated. An angular-correlation function is thus accumulated over many sweeps of the detection plane until the results are statistically significant. The electron-gun angle is then changed

and the whole procedure is repeated. Computer optimization of the analyzers allows for any small variation of their electrostatic imaging as they sweep around the detection plane, whereas the gun optimization allows for any long-term variation in the system operating conditions.

The movement of the electron gun, gas jet, and photomultiplier tube on a common axis ensures that the interaction volume as detected by the photomultiplier is accurately aligned to the center of rotation of the analyzers prior to evacuating the system, for all detection plane angles from coplanar geometry to the perpendicular plane geometry. Additionally, the flexibility of the experimental apparatus allows checks to be made on the reproducibility of the coincidence signal as the gun and analyzer angles are varied. In the perpendicular plane only the mutual angle ϕ is of importance and so the cross section is measured for constant ϕ as the analyzers sweep around this plane. The cross section is found to be independent of sweep angle, indicating that the overlap volume viewed by the detectors exceeds the interaction volume of the incident electron beam and gas jet, as required [3]. Away from the perpendicular geometry checks were made by measuring the coincidence signal for different detection energies $E_a = E_1$, $E_b = E_2$, and then remeasuring the signal with $E_a = E_2$ and $E_b = E_1$. The coincidence signals for each measurement were the same within the statistical accuracy of the measurements. As the apparatus cannot access gun angles ψ greater than 90° , checks on the reflection symmetry around this axis could not be made.

At an incident energy of 44.6 eV, the outgoing electrons were detected with equal energies $E_a = E_b = 10$ eV for nine gun angles [2] ψ from 0° to 90° . The results for 54.6-, 64.6-, and 74.6-eV incident energy were obtained also at symmetric energies $E_a = E_b = 15, 20,$ and 25 eV, respectively, using six gun angles $\psi = 0^\circ, 22.5^\circ, 45^\circ, 67.5^\circ, 80^\circ,$ and 90° . For gun angles ψ less than 70° the analyzers were constrained by the presence of the electron gun and Faraday cup to angles (ξ_a, ξ_b) between 35° and 125° , whereas for ψ between 70° and 85° the corresponding range was 35° to 140° . The perpendicular-plane geometry afforded the greatest angular freedom and the analyzers could move to angles (ξ_a, ξ_b) from 25° to 155° .

B. Normalization procedure at different incident energies and gun angles

Previous results [3] in the perpendicular plane were normalized to a common point by considering the relative efficiencies and detection solid angles of each analyzer together with the detected overlap volume at each energy. Those results, obtained from 10 to 80 eV above the ionization threshold, were then placed on an absolute scale using the coplanar results of Gélébart and Tweed [6]. Full details of the normalization procedure may be found in Ref. [3]. The same procedure has been used to place the present results on an absolute scale, since the differential cross section at $\xi_a = \xi_b = 90^\circ$ for all detection planes is the same as that in the perpendicular plane at the mutual angle $\phi = 180^\circ$. The estimated uncertainty in the absolute normalization is $\pm 44\%$.

C. Experimental results

Figure 4 shows the 44.6-eV data with the results at the lower gun angles on a logarithmic scale so that a comparison can be made between data at different incident energies, which is necessary since the variation in the cross sections at higher incident energies exceeds 2000:1. These 44.6-eV results have previously been presented on a linear scale [2] and so are only discussed briefly here. Figures 5, 6, and 7 show the results at 54.6-, 64.6-, and 74.6-eV incident energy, respectively, for $\psi=0^\circ$ and 22.5° [Fig. 4(a)], $\psi=45^\circ$ and 67.5° [Fig. 4(b)], and $\psi=80^\circ$ and 90° [Fig. 4(c)].

A notable feature present in the coplanar results ($\psi=0^\circ$) is the variation in the ratio of peak heights as the incident energy increases. The 44.6-eV data show a smaller forward-scatter peak compared with the backscatter peak as has been observed previously [10], the ratio of peak heights being 0.8:1. At 54.6 eV and above the

forward peak dominates over the backscatter peak, until at 74.6 eV the ratio of peak heights is 12:1. The minima between the lobes around $\xi=80^\circ$ appear to be stationary with increasing energy, while the ratio of forward maxima to interlobe minima varies from 3.0:1 at 44.6 eV to 140:1 at 74.6 eV.

As the gun angle ψ increases from 0° to 90° , the forward coplanar scattering peak is seen to evolve into the lower-angle perpendicular plane peak, whereas the backward-scattering peak evolves into the central perpendicular-plane peak. If the gun angle were to be increased further, from 90° to 180° , planar symmetry requires the present results to reflect through $\xi=90^\circ$ so that the backscatter peak would evolve into the forward-scatter peak and vice versa [see Eq. (5)].

The differential cross section is seen to vary slowly as the gun angle ψ increases to 22.5° (15° and 30° at 44.6 eV). A small change in the angle of the minimum is observed

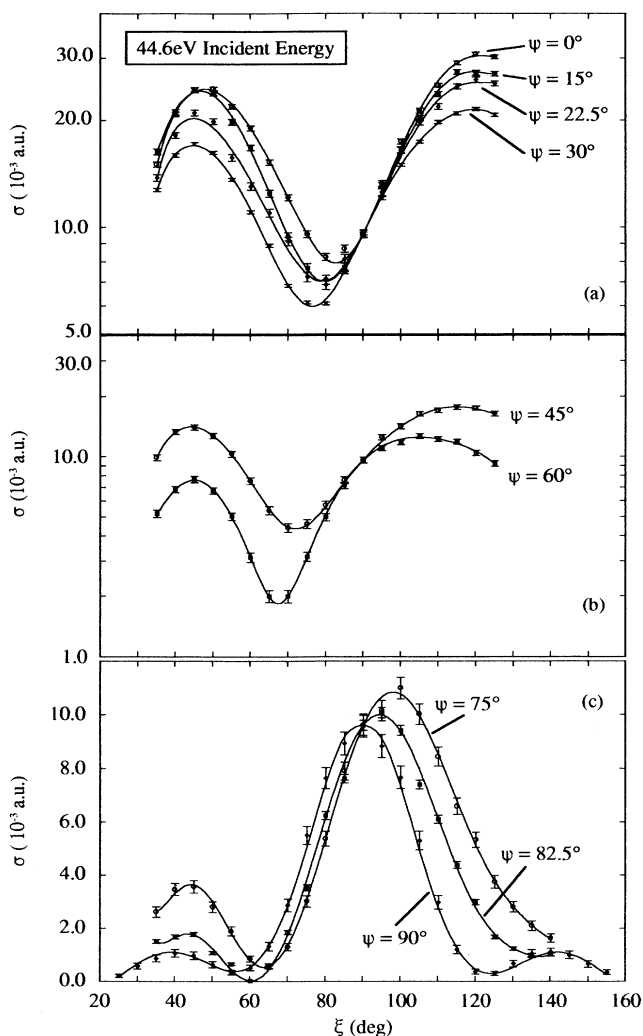


FIG. 4. (a)–(c) The absolute differential cross section of helium as a function of ξ and ψ at an incident energy of 44.6 eV, presented on a logarithmic scale [(a) and (b)] and a linear scale (c). The results are normalized to the common point at $\xi=90^\circ$, with an estimated uncertainty of $\pm 44\%$.

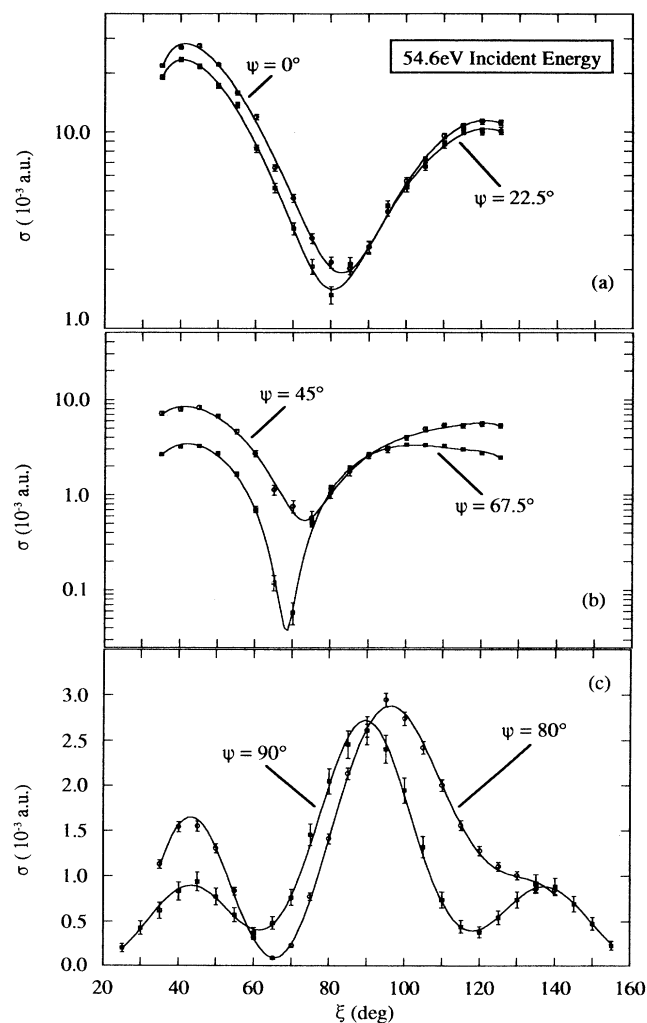


FIG. 5. (a)–(c) The absolute differential cross section of helium as a function of ξ and ψ at an incident energy of 54.6 eV, presented on a logarithmic scale [(a) and (b)] and a linear scale (c). The results are normalized to the common point at $\xi=90^\circ$, with an estimated uncertainty of $\pm 44\%$.

and the difference between the forward- and backward-scattering lobe intensity decreases. At $\psi=45^\circ$, the differential cross-section forward peak has decreased from the coplanar result by a factor of 5.2:1 at 74.6-eV incident energy, while the change in the backward scattered lobe is only 1.7:1 at this energy. The minimum in the differential cross section at $\psi=45^\circ$ has moved to $\xi \approx 75^\circ$ at all energies.

The differential cross section at $\psi=67.5^\circ$ (and to a lesser extent at $\psi=60^\circ$ at 44.6 eV) shows a deep minimum at $\xi \approx 70^\circ$ for all incident energies. As the forward- and backward-scattered lobe intensities are approximately equal at this gun angle, this deep minimum is possibly due to interference between the scattering amplitudes for the forward- and backward-scattering processes. In or-

der to elucidate the true depth of these minima, the experimental response function has been deconvolved from these results; the procedure for this deconvolution is presented in Sec. III D.

The results at $\psi=80^\circ$ and 90° (75° to 90° at 44.6 eV) have been plotted on a linear scale, since this enhances the observable effects at these higher gun angles. The forward-scatter peak is seen to evolve into the lower peak in the perpendicular plane, the backscatter peak evolves into the main central peak, and the higher angle wing evolves into the third perpendicular-plane peak. This latter effect is most visible at the highest impact energy, where it is observed that the evolution moves from a lower intensity in the wing to a higher intensity in the third perpendicular-plane peak at $\xi \approx 135^\circ$. It can be not-

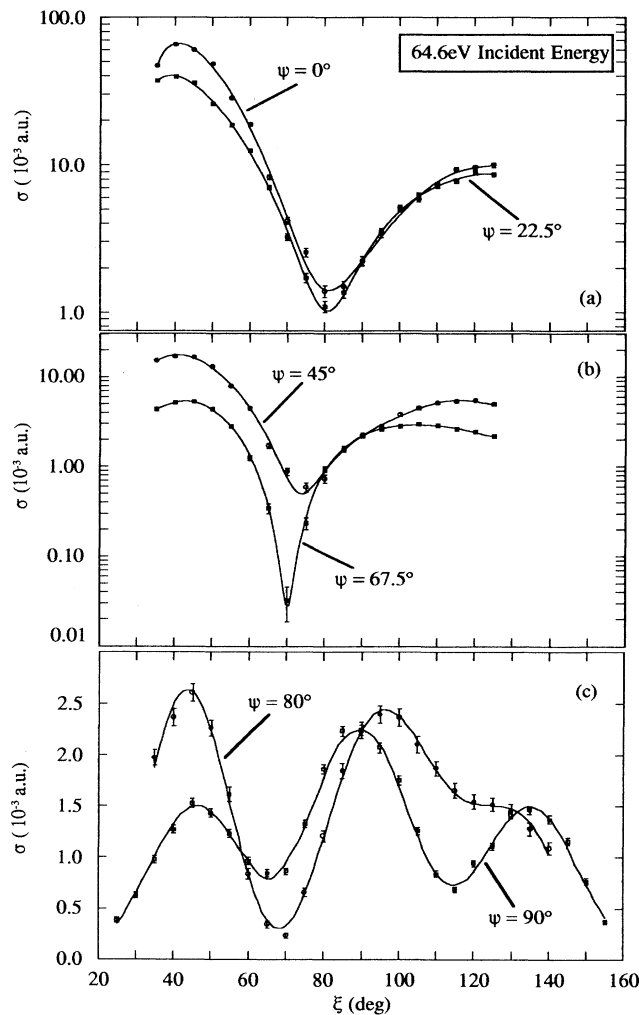


FIG. 6. (a)–(c) The absolute differential cross section of helium as a function of ξ and ψ at an incident energy of 64.6 eV, presented on a logarithmic scale [(a) and (b)] and a linear scale (c). The results are normalized to the common point at $\xi=90^\circ$, with an estimated uncertainty of $\pm 44\%$.

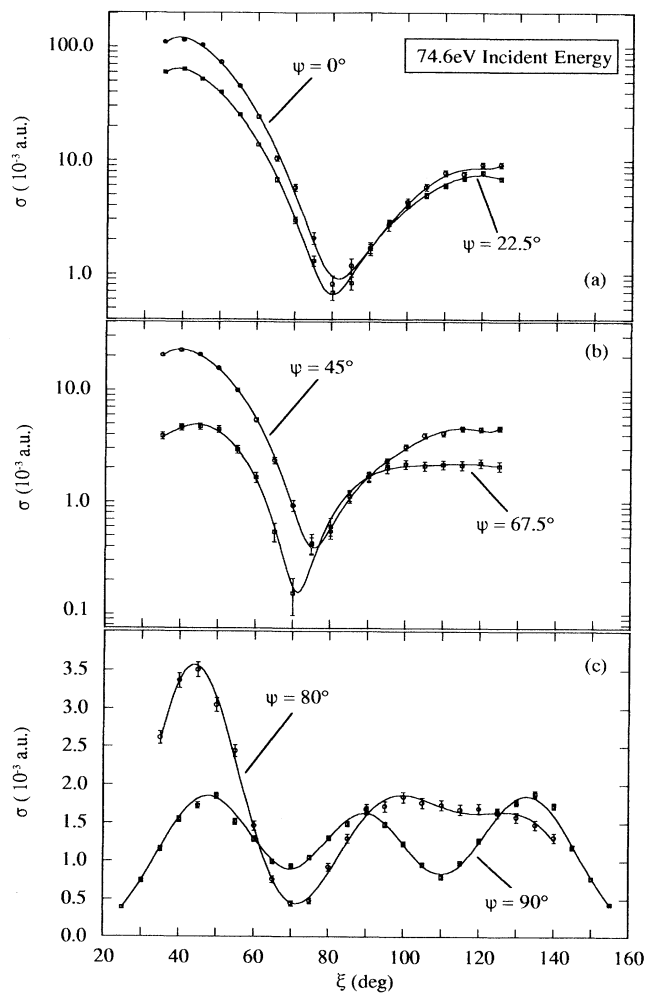


FIG. 7. (a)–(c) The absolute differential cross section of helium as a function of ξ and ψ at an incident energy of 74.6 eV, presented on a logarithmic scale [(a) and (b)] and a linear scale (c). The results are normalized to the common point at $\xi=90^\circ$, with an estimated uncertainty of $\pm 44\%$.

ed that the minima observed in the differential cross section for $\psi=67.5^\circ$ at incident energies of 54.6, 64.6, and 74.6 eV are deeper than the minima observed at $\psi=80^\circ$ and 90° . By contrast, at 44.6-eV incident energy, the minimum at $\psi=60^\circ$ is not as deep as those at higher gun angles. This effect may therefore be related to the mechanism that produces a forward peak that is smaller than the backscatter peak at this energy.

Finally, it can be noted that for each incident energy from 54.6 to 74.6 eV and for $\psi=45^\circ$ to 90° , the height of the forward peak is proportional to the Rutherford scattering factor $\text{cosec}^4(\psi/2)$ to within $\pm 10\%$. This may suggest that this yield results from scattering of the incident electron in the Coulomb field of the target nucleus, followed by a "binary" collision with the target electron.

D. Estimation of the depth of the minimum at $E_0=64.6$ eV and $\psi=67.5^\circ$

The measured differential cross section is the convolution of the experimental angular response function with the true differential cross section. The experimental response function is in turn a convolution of the angular acceptance of the analyzers together with the observed electron-beam pencil angle at the interaction region. It is possible to estimate the width and depth of the true differential cross-section minimum at $\psi=67.5^\circ$ by deconvolving the experimental response function from the measured data. To do this we assume that in the neighborhood of the dip the true differential cross section can be approximated by

$$\sigma_{\text{true}}(E_0, \xi, \psi) = \sum_{n=0}^k a_n(E_0, \psi) \xi^n, \quad (1)$$

where E_0 is the incident electron-beam energy and k is chosen to allow an accurate fit to the data. The angular response function of the apparatus is a convolution of the detection angles of the analyzers (half-angle approximately 3°) together with the beam angle of the incident electron beam (half-angle approximately 2°). Using the central limit theorem we approximate this to a Gaussian of

the form

$$f(\xi) = \frac{h}{\sqrt{\pi}} \exp(-h^2 \xi^2), \quad (2)$$

where the parameter h reflects the experimental angular full width w of the response function, estimated to be approximately 8° . The measured differential cross section is therefore given by

$$\sigma_{\text{meas}}(E_0, \xi, \psi) = \frac{h}{\sqrt{\pi}} \sum_{n=0}^k \int_{-\infty}^{\infty} a_n(E_0, \psi) (\xi')^n \times \exp\{-h^2(\xi - \xi')^2\} d\xi'. \quad (3)$$

This can be evaluated analytically to give

$$\sigma_{\text{meas}}(E_0, \xi, \psi) = \sum_{n=0}^k a_n g(\xi), \quad (4)$$

where

$$g(\xi) = \left\{ \xi^n + \sum_{j=1}^l \frac{n! \xi^{(n-2j)}}{j!(n-2j)! 2^{2j} h^{2j}} \right\}$$

and l is the integer part of $n/2$. The functions $g(\xi)$ can therefore be used as basis functions in a least-squares fit to the measured data to find the parameters $a_n(E_0, \psi)$. These parameters are then used in Eq. (1) to evaluate the true differential cross section prior to instrumental convolution.

A value of $k=9$ was found to give a good fit to the experimental data. The result of applying this deconvolution to the data at $E_0=64.6$ eV and $\psi=67.5^\circ$ is presented in Fig. 8 for various values of the width of the response function. It can be seen that as the width approaches the estimated value, the depth of the minimum rapidly decreases. It should be noted that the uncertainty in these fits increases as the minima deepen, since there is only limited experimental data around this point. A similar deconvolution applied to the results at the other incident energies indicates that although these minima deepen, they are not as deep as that at $E_0=64.6$ eV.

This behavior is consistent with the suggestion given above that the dip is due to interference between the forward- and backward-scattering amplitudes, since at this incident energy the forward and backward peak yields are approximately the same. The high order of symmetry of the experiments presented here might also contribute to the extent of the deep minimum at $E_0=64.6$ eV. Experiments where the scattering symmetry is relaxed are currently being undertaken to test this hypothesis.

E. Three-dimensional surfaces representing the differential cross section

The range of experimental geometries used in the present study allows a three-dimensional (3D) map of the differential cross section to be produced in a way similar to that in which the angular description of electron-impact-excited valence states are obtained from electron-

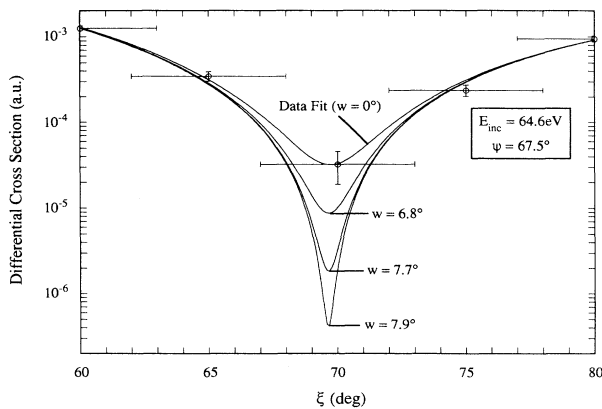


FIG. 8. The estimated differential cross section at $E_0=64.6$ eV and $\psi=67.5^\circ$ indicating the depth of the minimum when the experimental response function is deconvolved from the measured differential cross section. See the text for details.

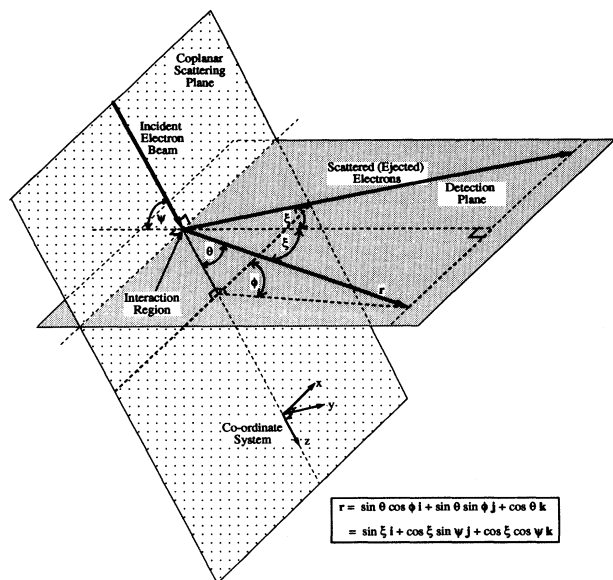


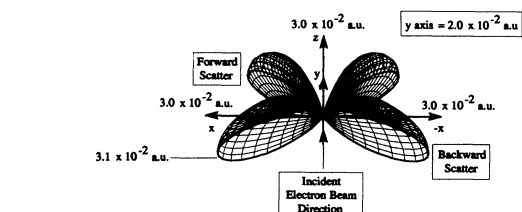
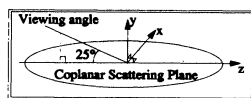
FIG. 9. The transformation between the angles (ξ, ψ) and the spherical polar angles (θ, ϕ) .

photon correlation studies [11]. This is possible since measurements in a given detection plane characterize a two-dimensional “slice” of the total differential cross section [2]. The doubly symmetric differential cross section possesses two planes of reflection symmetry due to the unpolarized state of the atomic beam and the indistinguishability of the detected electrons. One of these planes is the detection plane and the other is the plane of the rotating incident electron beam. A further symmetry that can be used to generate results for $\psi=90^\circ$ to 180° is given by

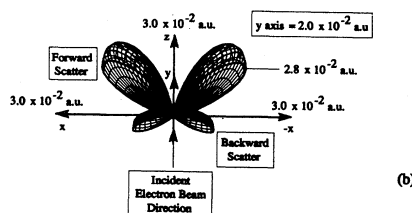
$$\sigma(180^\circ - \xi, 180^\circ - \psi) = \sigma(\xi, \psi). \quad (5)$$

Reflection symmetry around $\xi=0^\circ$ in the detection plane indicates that an expansion in powers of $\cos \xi$ can be used to parametrize the differential cross section at constant ψ . The parametrization was additionally constrained to yield zero cross section at $\xi=0^\circ$ and 180° for all angles ψ due to post-collisional repulsive interactions between the outgoing electrons.

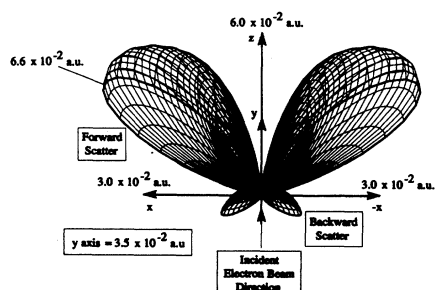
A good fit to the data for all detection planes ψ_i ($i=1, \dots, n$, where n is the number of detection planes at a particular incident energy) was obtained by including



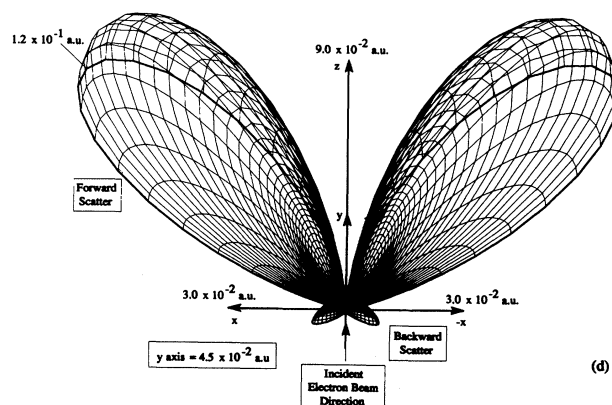
(a)



(b)



(c)



(d)

FIG. 10. (a)–(d) 3D differential-cross-section surfaces “doubly symmetric” in scattering angle and energy for incident electron energies from 44.6 to 74.6 eV, parametrically calculated from the results presented in Figs. 4–7. The view is directed along the $+z$ incident electron direction at an angle of 25° to the $(x-z)$ plane (see inset). The axes are linear and extend to 3.0×10^{-2} a.u. in the $\pm x$ directions and as shown in the $+y$ and $+z$ directions. The maximum in the cross section is indicated for the coplanar geometry in each case. The coplanar geometry yield is highlighted and the noncoplanar yield is shown for positive values of y only.

nine terms in the parametrization. Thus,

$$\sigma(E_{\text{inc}}, \xi, \psi_i) = \sigma(E_{\text{inc}}, \xi = 90^\circ) + \sum_{j=1}^9 b_j(\psi_i) \cos^j(\xi). \quad (6)$$

The parameters $b_j(\psi_i)$ ($j=1..9$) were then fitted to a polynomial in $\cos(\psi)$ over the range of angles $\psi_i=0^\circ$ to 90° , yielding fitting parameters c_{ji} characterizing the total differential cross-section surface. Thus,

$$\sigma(E_{\text{inc}}, \xi, \psi) = \sigma(E_{\text{inc}}, \xi = 90^\circ) + \sum_{i=0}^{n-1} \sum_{j=1}^9 c_{ji} \cos^i(\psi) \cos^j(\xi). \quad (7)$$

This form satisfies relationship (5) and so was used to generate the fit for ψ ranging from 90° to 180° . Finally, the fitted differential cross section, a function of the detection plane angle ξ and gun angle ψ , was remapped into the conventional coordinate system as defined in Fig. 1. Using unit vectors ($\mathbf{i}, \mathbf{j}, \mathbf{k}$) along the x , y , and z axes as shown in Fig. 9, a general unit vector \mathbf{r} can be expressed in terms of either (ξ, ψ) or (θ, ϕ) as follows:

$$\begin{aligned} \mathbf{r} &= \mathbf{i} \sin\theta \cos\phi + \mathbf{j} \sin\theta \sin\phi + \mathbf{k} \cos\theta \\ &= \mathbf{i} \sin\xi + \mathbf{j} \cos\xi \sin\psi + \mathbf{k} \cos\xi \cos\psi. \end{aligned} \quad (8)$$

Therefore,

$$\tan\phi = \cot\xi \sin\psi, \quad (9)$$

$$\cos\theta = \cos\xi \cos\psi. \quad (10)$$

Figures 10(a)–10(d) illustrate the 3D surfaces generated from this parametrization for the incident energies from 44.6 to 74.6 eV. In this example each differential cross section surface is viewed at an angle of 25° to the incident electron-beam direction and is plotted on the same linear scale to allow direct comparison at the different incident energies. The differential cross section surface is only shown above the coplanar scattering plane, since reflection symmetry dictates that the surface is identical below this plane. The coplanar differential cross section yield is highlighted in each of the figures.

The differential cross section surfaces are seen to have reflection symmetry in the y - z (gun angle) plane, which is necessary because of the equivalence of the detected electrons. At an incident energy of 44.6 eV, the 3D differential cross section surface is seen to have a forward lobe that is smaller than the lobe in the backscatter direction, as noted in Fig. 4. At 54.6 eV the overall differential cross section surface has reduced in volume, and the forward lobe dominates over the backscatter lobe. As the incident energy increases further, the differential cross section expands rapidly in the forward direction, while the backscatter lobe area varies only slowly with increasing energy. Finally it can be noted that the normalization point along the x axis is largest at 44.6 eV, and decreases as the incident energy is increased, as has been noted previously [3].

The evolution from the coplanar forward- and backward-scattering lobes into the three perpendicular-plane lobes is difficult to see in these figures since the relative height of the backscatter surface tends to mask these effects. This evolution can be seen more clearly in Fig. 3 of Ref. [2], where the 3D differential cross section surface at 44.6 eV is shown rotated around the y axis.

We present the three-dimensional representation of Fig. 10 because it indicates that the differential cross section measurements at incident energies of 54.6, 64.6, and 74.6 eV form a natural sequence, while those at 44.6 eV appear to be significantly different in form. This in turn might indicate that there are correlation, distortion, capture, or exchange processes that are significant only at incident energies below about 50 eV.

IV. COMPARISON WITH THEORETICAL CALCULATIONS

Few theoretical calculations exist for noncoplanar geometries at these incident energies. The perpendicular-plane results have been modeled using a second-order Born approximation [12] and a distorted-wave Born approximation [13]. Coplanar symmetric results [10], which straddle the present coplanar results at an incident energy of 44.6 eV, have been modeled using a distorted-wave calculation [14], but the experimental results are not reproduced even qualitatively. Recent theoretical work [15] has made considerable progress toward modeling these experimental results at the lower energy range from 0.5 to 5 eV above threshold, by including a normalization factor in the Coulomb-Born approximation [16] that incorporates final-state electron-electron interactions. This agreement between theory and experiment indicates the importance of including these correlations in the model. As far as the authors are aware, no theoretical results exist with which to compare the three-dimensional differential-cross-section surfaces presented here.

V. CONCLUSION

Angular-correlation studies for the electron-impact ionization of a helium target from the coplanar geometry to the perpendicular-plane geometry have been presented at four different incident energies. The electrons were detected symmetrically in both energy and scattering angle, the results being collected using a fully computer-controlled and real-time computer-optimized ($e, 2e$) spectrometer. The ($e, 2e$) differential cross sections are placed on an absolute scale using the coplanar results of Gélébart and Tweed [6].

These measurements couple differential cross sections obtained in coplanar geometry to those obtained in the perpendicular plane, and have been carried out at four different energies from 20 to 50 eV above the helium ionization threshold. A deep minimum is observed in the cross section at an intermediate plane given by $\psi=67.5^\circ$, and this is found to approach zero at an incident energy of 64.6 eV. The full differential cross section surface with

respect to a chosen scattering plane can therefore be modeled, and examples of these surfaces have been presented. At present no theoretical results exist with which to compare these three-dimensional differential-cross-section measurements.

ACKNOWLEDGMENTS

The U.K. Science and Engineering Research Council is gratefully acknowledged for their financial support for this work and for A. J. M. during this period.

-
- [1] A. Lahmam-Bennani, *J. Phys. B* **24**, 2401 (1991).
 - [2] A. J. Murray and F. H. Read, *Phys. Rev. Lett.* **69**, 2912 (1992).
 - [3] A. J. Murray, M. B. J. Woolf, and F. H. Read, *J. Phys. B* **25**, 3021 (1992).
 - [4] T. J. Hawley-Jones, F. H. Read, S. Cvejanovic, P. Hammond, and G. King, *J. Phys. B* **25**, 2393 (1992).
 - [5] T. Rösel, J. Röeder, L. Frost, K. Jung, H. Ehrhardt, S. Jones, and D. Madison, *Phys. Rev. A* **46**, 2539 (1992).
 - [6] F. Gélébart and R. J. Tweed, *J. Phys. B* **23**, L641 (1990).
 - [7] F. H. Read, in *Electron Impact Ionization*, edited by G. Dunn and T. Märk (Springer, Berlin, 1985), pp. 42–88.
 - [8] A. J. Murray, B. C. H. Turton, and F. H. Read, *Rev. Sci. Instrum.* **63**, 3349 (1992).
 - [9] J. A. Nelder and R. A. Mead, *Comput. J.* **7**, 308 (1965).
 - [10] T. Rösel, C. Dupré, J. Röeder, A. Duguet, K. Jung, A. Lahman-Bennani, and H. Ehrhardt, *J. Phys. B* **24**, 3059 (1991).
 - [11] N. Andersen, J. W. Gallagher, and I. V. Hertel, *Phys. Rep.* **165**, 1 (1988).
 - [12] F. Mota-Furtado and P. F. O'Mahony, *J. Phys. B* **22**, 3925 (1989).
 - [13] X. Zhang, C. T. Whelan, and H. R. J. Walters, *J. Phys. B* **23**, L173 (1990).
 - [14] C. T. Whelan, X. Zhang, and H. R. J. Walters (unpublished).
 - [15] J. Botero and J. H. Macek, *Phys. Rev. Lett.* **68**, 576 (1992).
 - [16] J. Botero and J. H. Macek, *J. Phys. B* **24**, L405 (1991).